MMT-AO: two years of operation with the first adaptive secondary

G. Brusa[a], D. L. Miller[a], M. Kenworthy[a], D. Fisher[a], A. Riccardi[b]

[a] Steward Observatory/Univ. of Arizona, 933 Cherry Av., Tucson AZ, 85721, USA
[b] INAF-Osservatorio Astrofisico di Arcetri, L.go E. Fermi 5, 50125 Firenze, Italy

ABSTRACT

The Multiple Mirror Telescope (MMT) adaptive optics system (MMT-AO) has been operated in a campaign mode for the last two years. In total seven runs, each lasting about two weeks, have been carried out. During these observational runs a large amount of data have been collected. These data allow us to draw some preliminary conclusions about the overall system performances. In this paper we discuss in detail the achieved performances of the MMT-AO system which is equipped with the first adaptive secondary ever developed. The performances are examined both in terms of number of corrected modes and control bandwidth achieved. We also discuss our attempts to improve the system calibration. This is done by modulating the internal slope offsets while the system is operating in closed loop on the sky.

Keywords: adaptive optics, deformable mirrors, adaptive secondary mirrors, electromagnetic actuators, capacitive sensors

1. INTRODUCTION

The Multiple Mirror Telescope (MMT) adaptive optics system (MMT-AO) has been operated in a campaign mode for the last two years. In total seven runs, each lasting about two weeks, have been carried out. During these observational runs a large amount of engineering data have been collected. These data allow us to characterize the performance of the entire system and the various sub-systems. One of the key components is the adaptive secondary. This is the first ever developed and used on the sky. The characterization of the MMT adaptive secondary was started several years ago and many results have already been published. In particular: for a description of the unit and a discussion of the electro-mechanical aspects readers should refer to Ref. 1 (and references therein), for the details about the more recent developments and the integration in the MMT-AO we point to Ref. 2, 3.

Here we will be concerned with some aspects of the operation of the adaptive optics system that are peculiar to the use of the adaptive secondary as well as some quantification of the performances achieved. Other two papers presented at this conference discuss the project status and future developments[4] and science results.[5]
In Sec. 2 we give a general description of the main AO components and describe a basic model for it. In Sec. 3 we describe how the optical interaction matrix of the system was measured in the lab and how from this matrix the various reconstruction matrices are computed. In Sec. 4 we introduce a technique that was used to check the current calibration of the AO system. This technique which we call loosely "reconstructor on the sky" allows us to determine if there is any difference between the optical interaction matrix that describes the system at the telescope and the one measured in the lab more than two years ago. Using this technique we can also determine the effect of the seeing variability on the total system gain and therefore on the closed loop bandwidth. Finally, in Sec. 5 we report on the effect of relatively high ($6 - 80\,Hz$) vibrations of the front end structure of the telescope that prevents achieving with long exposures the strehls (see Ref. 3, 5) obtained with short exposures (few ms).

Further author information: (Send correspondence to G.B.)
G.B.: E-mail: gbrusa@as.arizona.edu, Telephone: +1 520 626 9529

Advancements in Adaptive Optics, edited by Domenico Bonaccini Calia, Brent L. Ellerbroek, Roberto Ragazzoni, Proceedings of SPIE Vol. 5490 (SPIE, Bellingham, WA, 2004)
0277-786X/04/$15 · doi: 10.1117/12.552513

Figure 1. The adaptive secondary installed at the MMT telescope. In the foreground the telescope structure, in the background the Arizona desert south of Tucson. This photo was taken during the Jan-Feb 2004 run.

2. AO SYSTEM DESCRIPTION

2.1. Introduction

In Fig.2 we show a diagram of the AO system. The main components are: the wavefront sensor (WFS) (a 12x12 sub-aperture Shack-Hartmann, see Ref. 6) , the adaptive secondary (AS) and the wavefront computer (WFC). The WFC is a real-time system composed of essentially five blocks: the wavefront sensor interface ($WFSI$), the sub-aperture slope computer (SSC), the real-time reconstructor (RTR), the deformable mirror interface (DMI) and the diagnostic data storage (DDS). The DDS allows saving various data to perform diagnostic and performance analysis. There are six type of data that can be saved and these are (proceeding from the WFS toward the AS):

- *spo*, the WFS camera frames;
- *slo*, the computed slopes plus any slope offset;
- *rtr*, the reconstructed mirror delta commands;
- *com*, the mirror commands;
- *pos*, the mirror positions;
- *cur*, the mirror currents.

The maximum number of time samples that can be saved if all the data types are saved is currently 4000. This at the highest sampling rate ($550\,Hz$) correspond to $\simeq 7.3$ seconds of continuous data. Some of these data are redundant and in fact to analyse the AO performances only the *slo* data (with some additional auxiliary data) are needed, in this case time sequences up to 12000 samples can be saved.

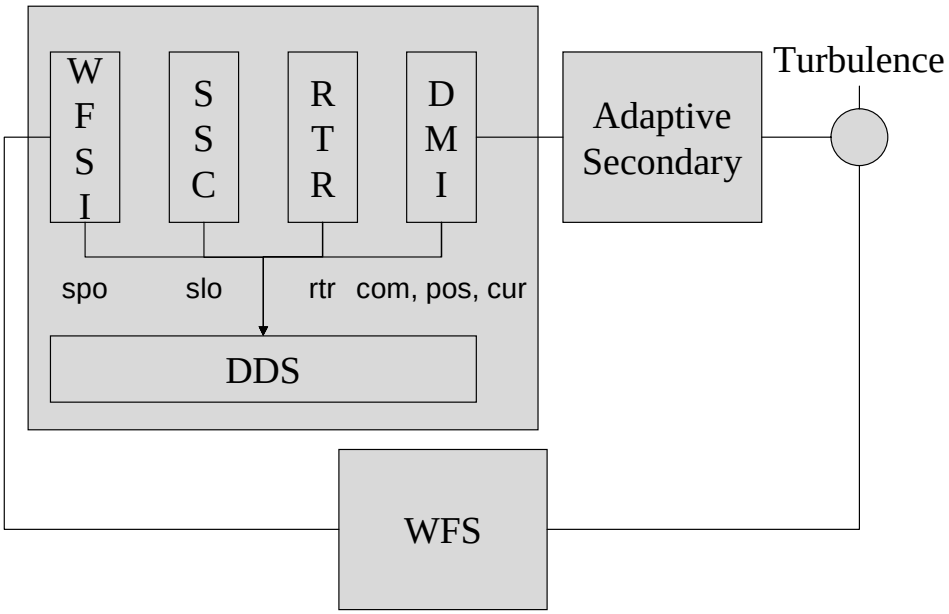

Figure 2. Block diagram of the MMT-AO system. See Sec.2.1 for explanation of the various components.

2.2. System model

In Fig.3 a block diagram of the basic functions performed by the system is shown together with the notation for operators and signals used in this paper. For the signals we have: t input wavefront, s_{in} calculated slopes (from WFS frames), s_{out} total slopes, s_{off} slopes offsets, *com* mirror commands and *pos* mirror positions. We remind that the various signals belong to different spaces. In particular: t belongs to the space of wavefronts (continuous functions over the system's pupil), s_{in}, s_{off} and s_{out} are in the space of WFS slopes ($nslo \leq 108 \times 2$) and *com* and *pos* are in the space of the mirror actuators ($nact = 336$). The operators may involve both a time filtering and a space transformation. In particular: WFS performs a time filtering ($g^{'}(r_0)\, h_{wfs}$) and a transformation from continuous space to slopes (indicated by D_∞), REC performs a transformation from the space of slopes to actuator space, h_c is the time filtering introduced to compensate the loop delay (a simple integrator in our case), h_{dm} takes into account the mirror time response (and is assumed to be independent of the particular mirror command). In theory we should also introduce an operator that converts from mirror *pos* (a vector of size *nact*) into actual wavefront but since there is a direct correspondence (provided by the mirror thin shell) this has been omitted.

We point out that the operation associated to the WFS block is in fact quite involved, in fact WFS camera frames are used to produce a quad-cell signal associated with each active sub-apertures which is then linearized thru the use of a look-up table (LUT). Finally, the factor $g^{'}(r_0)$ is introduced to take into account the change in gain due to spot blurring at the sub-aperture level. This blurring is seeing dependent, thus the dependency from r_0, the seeing coherence diameter.

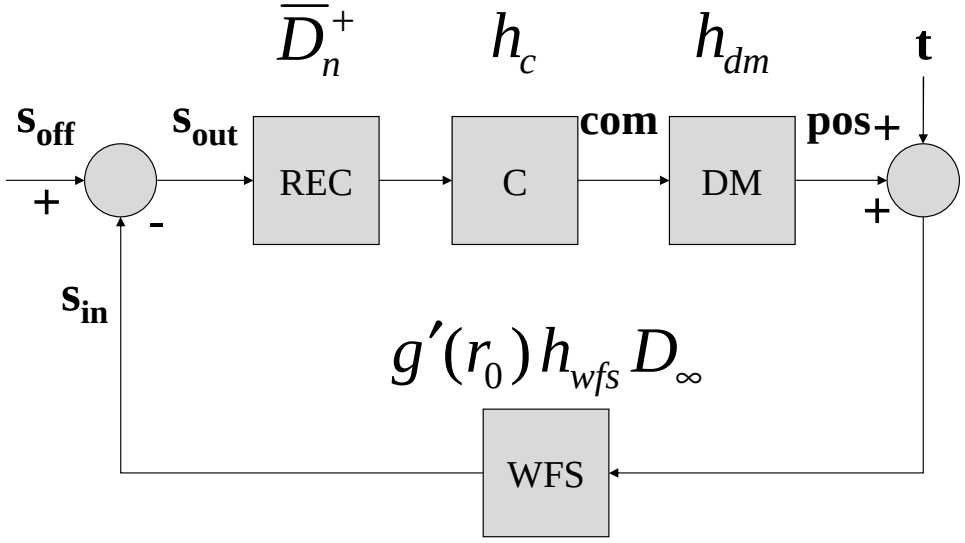

Figure 3. Diagram of the MMT-AO system model. In this diagram emphasis is put on the two system inputs: the slope offsets s_{off} and the input wavefront t.

3. WAVE-FRONT RECONSTRUCTION

3.1. Interaction matrix

This measurement is done generally by applying mirror deformations and recording the effect produced on the wave-front sensor. In our case the mirror deformations are defined by the vector of actuator displacements applied by the adaptive secondary and the wave-front sensor measurements are the delta slopes recorded with the Shack-Hartmann based wavefront sensor. The mirror data are vectors of size *nact* and the sensor data are vectors of size *nslo*. The interaction matrix is thus a matrix D of size $nslo \times nact$. An interaction matrix can be built by applying any set of deformations provided that their span is the space that we are trying to characterize. The acquisition of the data used to build the interaction matrix was done in the laboratory more than two years ago (Feb. 2002) and never repeated since then. In fact this measurement must be done by directly illuminating the adaptive secondary and the projecting optics used in the lab (see Ref.2) was never installed at the telescope. For this measurement we used the set of feed-forward (FF) modes.[1] The feed-forward matrix (FFM) is the linearization (around the particular operating condition) of the relationship between static actuators currents and actuators displacements. The singular values associated with the FFM provide an ordering based on rms current required per unit rms displacement. Since there is a linear relationship between actuator current and actuator force these modes are also ordered according to rms force.
The basic statics equation for a thin plate (to which our shell can be assimilated with good approximation) show that the force required to bend the plate scales as k^4 where k is the wavenumber associated with the deformation. On the other hand the signal measured by the SH only increases as k; it is then natural to start measuring first

the modes that are easier to deform. In fact in the lab only the first 120 FF modes were used since these cover most of the turbulence 'seen' by the SH (see for instance Ref.7).
Here we also point out that a selection of 'illuminated' sub-apertures must be done. Given our geometry of the 144 sub-apertures availables only 108 are considered 'illuminated' (flux $\geq$ 50% of the fully illuminated ones). In our case, moreover, because of some local defects present in four locations of the AS surface (see Ref.2) we usually discard five more sub-apertures leaving a total of 103 'active' sub-apertures.

3.2. Reconstruction matrix

The reconstruction is performed using a least squares solution, i.e. given the measured slopes *slo* we find a set of mirror displacements *pos* such that the variance of the difference $slo - D\,pos$ is minimized. In general the solution can be found by computing the pseudo-inverse of D with an SVD algorithm. In practice more than one reconstructor is needed according to the order of the correction that is implemented, this is generally referred as modal filtering. So far we have experimented with a basic version of modal filtering where the modal gains are either 1 or 0. To build an order n reconstructor we proceed as follows:

- An SVD decomposition of the interaction matrix of order m, D_m, with $m >= n$ is computed;
- the computed singular vectors are ordered according to increasing singular value;
- a pseudo-inverse D_n^+ is computed directly from the SVD decomposition of D_m in the following way: the mode with the lowest singular value is filtered out (this is essentially a piston mode) and all the modes above n are also filtered out.

In practice to build a reconstructor of order n we always use m=n, in other words we always use the lowest possible order of the interaction matrix. This is because of two reasons:

- higher order Ds are affected by larger errors that then propagate into the reconstructor;
- because of the lack of symmetry due to the 'bad' sub-apertures higher order Ds produce asymmetric modes which have higher noise propagation factors.

So far only 56 and 80 modes (this is the order n) reconstructors have been extensively used at the telescope. Based on the data collected of the corrected PSF we don't find a significant difference in performances between the two reconstructors, when bright ($M_V \leq 10$) reference stars are used.

4. RECONSTRUCTOR CALIBRATION ON THE SKY

In Sec.1 we mentioned the fact that no direct calibration of the interaction matrix can be performed currently at the telescope. In order to check the quality of the reconstuctor used we devised a technique that in principle allows us to refine the current reconstructor. This technique uses data acquired with the system operating in closed loop on the sky. In short we use a temporal modulation of the slope offsets s_{off} to estimate the interaction matrix; this can be retrieved by performing a linear fitting over the slope data acquired during modulation. We want to point out that of course since this technique uses closed loop data, an initial approximation of the interaction matrix must be available. Moreover the accuracy of this fitting is limited by the presence of noise generated by the concurrent correction of the turbulent signal.

4.1. Basic equations

The main equation that will be used in the following can be derived from the system model shown in Fig.3. This relates the signal s_{in} or the slopes measured by the wavefront sensor to the turbulence signals t and the slope offset signal s_{off} (which is set by the user). In the transformed variable domain ω we have:

$$(1 + h_{ol}\, D_\infty\, \overline{D}_n^+)\, \tilde{s}_{in} \;=\; g^{'}\, h_{wfs}\, D_\infty\, (\tilde{t} \,+\, h_{dm}\, h_c\, \overline{D}_n^+\, \tilde{s}_{off}) \qquad (1)$$

where the tilde indicates the Fourier transform, $h_{ol} = g^{'}(r_0)\, h_{wfs}\, h_{dm}\, h_c$ and the overline has been used in $\overline{D}_n^+$ to indicate that this is the reconstructor derived from lab data, in principle different from the actual one. In this equation the wavefront sensor noise has not been included, under the assumption that it is negligible. In this case, assuming to know the various time filtering functions, the matrix D_∞ restricted to the range of $\overline{D}_n^+$ can be fitted from Eq.1. This is more clear if we rewrite Eq.1 as follows where we also specialized the equation for $\omega = \omega_{off}$, the pulsation of the slope modulation:

$$-\, g^{'}\, h_{wfs}(\omega_{off})\, D_\infty\, \tilde{t}(\omega_{off}) + \tilde{s}_{in}(\omega_{off}) \;=\; h_{ol}(\omega_{off})\, D_\infty\, \overline{D}_n^+\, \tilde{s}_{out}(\omega_{off}) \tag{2}$$

here $\tilde{s}_{in}(\omega_{off})$ and $\tilde{s}_{out}(\omega_{off})$ are the two measured quantities and the first term on the left is the noise term. The noise term can be estimated using the spectrum of s_{in} at some pulsation $\omega^{'}$ near ω_{off}, from Eq.2 we derive:

$$g^{'}\, h_{wfs}(\omega^{'})\, D_\infty\, \tilde{t}(\omega^{'}) \;\cong\; (1 + h_{ol}(\omega^{'})\, \overline{D}_n\, \overline{D}_n^+)\, \tilde{s}_{in}(\omega^{'}) \;=\; \tilde{s}_{in}^{\perp} \;+\; (1 + h_{ol}(\omega^{'}))\, \tilde{s}_{in}^{\parallel} \tag{3}$$

where in the first equation $D_\infty\, \overline{D}_n^+$ was approximated by $\overline{D}_n\, \overline{D}_n^+$ and the symbols $\perp$ and $\parallel$ indicate respectively the components along the kernel of $\overline{D}_n^+$ and along its complement.

4.2. Data acquisition

To proceed in practice we chose the set of right singular vectors of $\overline{D}_n^+$ as slope modulation vectors. As discussed in Sec.3 $\overline{D}_n^+$ does not have full rank since it is obtained using only the first n feed-forward modes. In fact its rank is exactly n-1, the number of reconstructed modes. The operation involved in the acquisition of the data consists in the following:

- a non zero singular value of $\overline{D}_n^+$ is chosen;
- the corresponding right singular vector is applied as slope offset s_{off} with a sinusoidal time modulation at pulsation ω_{off} ;
- a sequence of *slo* (with some auxiliary data) is saved in the DDS;
- the operation is repeated until all the non zero singular values have been acquired.

4.3. Data analysis

An example of the data obtained on the sky is shown in Fig.4. On the left the signal $\tilde{s}_{in}$ projected on mode#0 * is plotted as a function of time frequency. In this case a modulation $\tilde{s}_{off}$ of mode#0 at frequency 11Hz had been applied and the signal is clearly visible on top of the noise generated by the turbulence. In Fig.4(right) the component $\tilde{s}_{in}$ projected on mode#43 for the same case shows that there is some cross-coupling between mode#0 and this particular mode.

The analysis has to be performed considering the signal to noise achieved, this is shown in Fig.5 where all the modes are shown at the particular frequency of the modulation. In principle a new estimate for $\overline{D}_n$ can be obtained by performing a linear fitting on the data obtained for all the applicable modes. This was attempted for a 56 modes reconstructor last February with mixed results. It is clear that in any case if there is an improvement to be done on the matrix it is small. On the other hand it seems that the propagation of the noise even at low levels affect the fitting. There is also a general question about these data: are we seeing a cross-coupling or is it may be a non-linear effect due to the fact that our SH sensor uses quad-cells?

One interesting by-product of this technique is the direct determination of the value of $g^{'}$. Eq.2 can be rewritten projecting along the right singular vectors of $\overline{D}_n^+$. In this case if we only consider the component along the vector that is being modulated we have:

$$\tilde{s}_{in}^{*}(\omega_{off}, i_{off}) \;\cong\; h_{ol}(\omega_{off})\, \tilde{s}_{out}^{*}(\omega_{off}, i_{off}) \tag{4}$$

*In the following for sake of compactness we will sometime use 'modes' instead of 'right singular vectors of $\overline{D}_n^+$'.

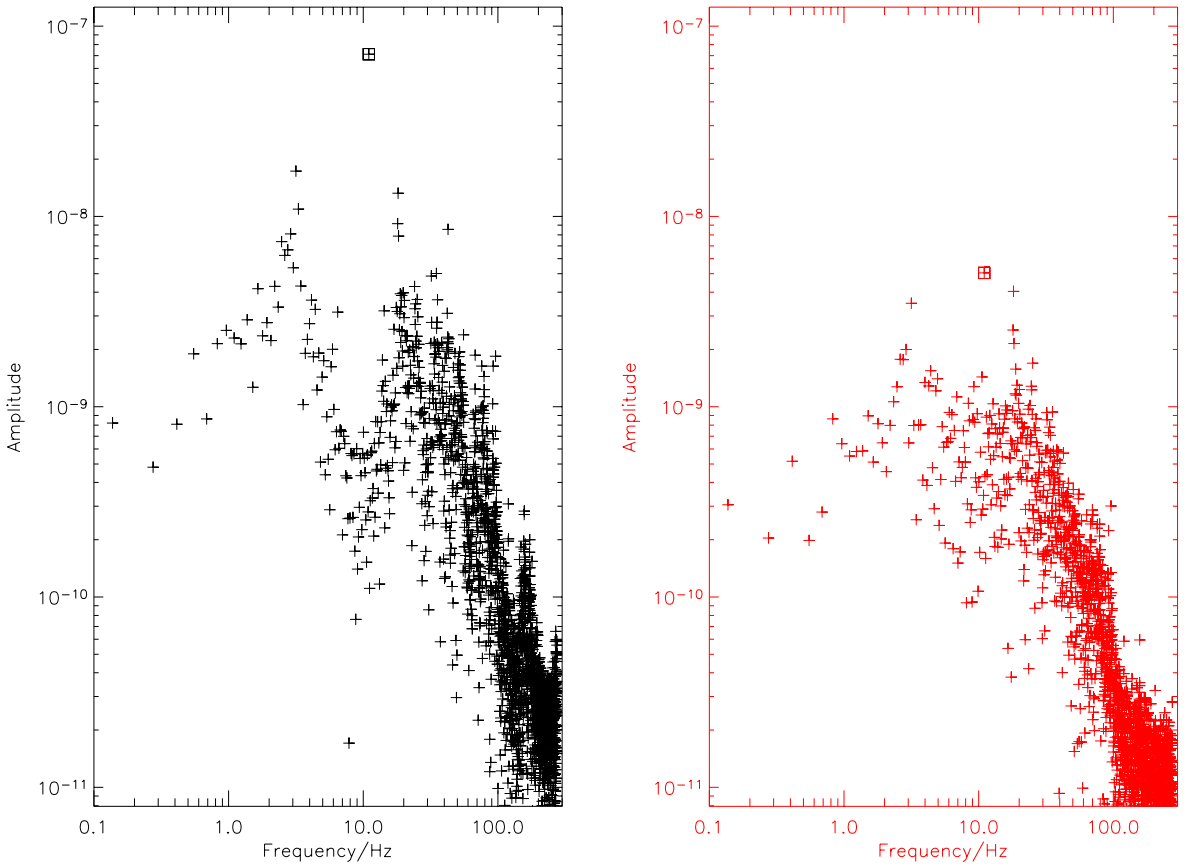

Figure 4. (Left) Amplitude of the signal $\tilde{s}_{in}$ projected along mode#0 as a function of frequency. (Right) Amplitude of the same signal projected along mode#43. A cross-coupling of about 6% is visible.

where $\tilde{s}^*(\omega_{off}, i_{off})$ is the component in the direction of the singular vector i_{off} at the pulsation ω_{off}. In Eq.4 the contribution of the turbulence has been neglected and $D_\infty \overline{D}_n^+$ has been approximated by the identity matrix. Since $h_{ol}(\omega_{off})$ is supposed to be known except for the factor $g^{'}(r_0)$, this latter can be easily retrieved . In Fig.6 a plot of the computed $g^{'}$ as a function of time is shown in comparison with an estimate of the seeing angle (λ/r_0). The value of r_0 is estimated from the same data by fitting the reconstructed open loop data to Zernike polynomial (see Ref.3). In Fig.6 (right) the value of $g^{'}$ vs. r_0 is shown for the same data set. the correlation between the two parameters is evident.

5. RESIDUAL TIP-TILT ERROR

In this section we characterize the residual tip-tilt jitter after AO correction. This error seems to be the largest in the overall budget and is the first that we plan to tackle in the near future. What was found is that while the AO system performs as expected in correcting the turbulence contribution of the tip-tilt error, it is not able to correct terms introduced by telescope structure vibrations. These vibrations are in the frequency range of $6 - 80\,Hz$ which falls only partially within the rejection bandwidth of the AO system.

5.1. A specific case

In order to illustrate the problem we chose a specific case were in addition to WFS measurements direct PSF measurements taken with an engineering camera operating in the $H - band$ were available. During this short

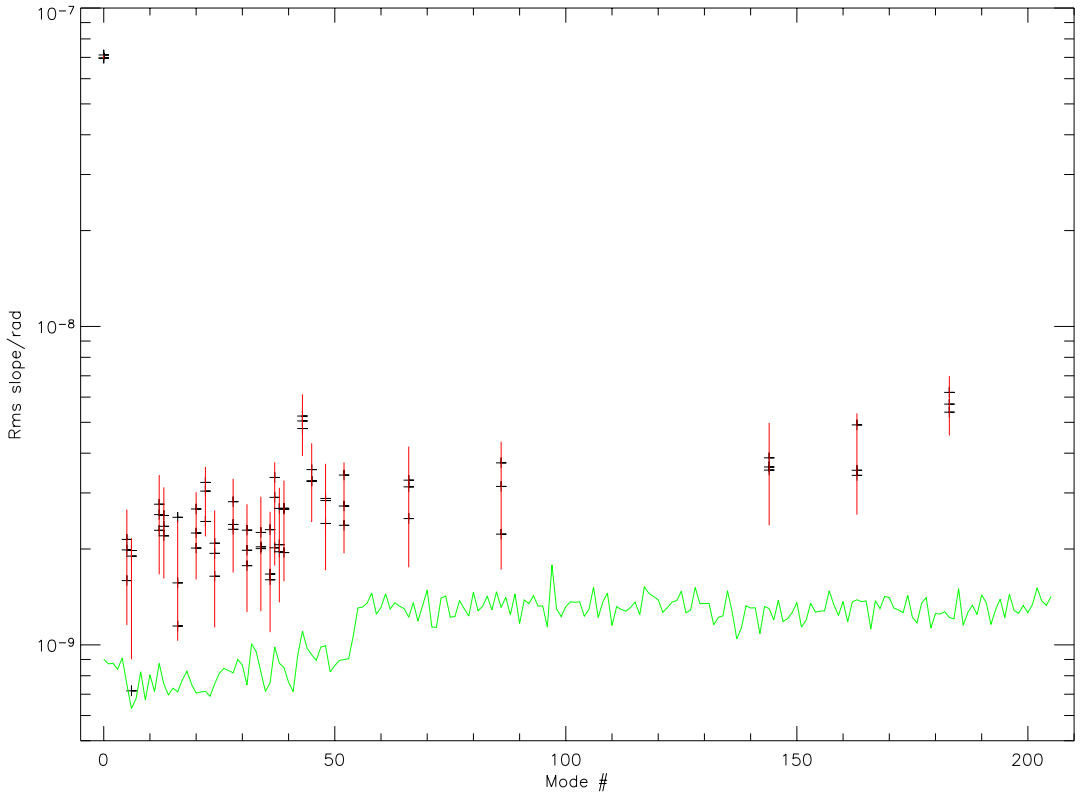

Figure 5. Decomposition of the signal $\tilde{s}_{in}(\omega_{off})$ along all the modes. In this case mode#0 was applied to the s_{off} signal with a pulsation ω_{off} corresponding to 11Hz. The solid line represents the noise estimated at $\omega^{'}$ near ω_{off}. For clarity only the modes with a signal to noise greater than two are shown. A total of three measurements were done indicated by the short horizontal bars.

set of tests the seeing was ($\cong$ 0.6") and we had average wind conditions. Most of the PSF measurements gave a Strehl of $30-40\,\%$ for the short exposure case (integration of a few ms) and a long exposure Strehl of $\leq 20\%$. This reduction in Strehl can be explained by the residual uncorrected tip-tilt term. In Fig.7 the residual closed loop cumulative variance for both tip and tilt as seen by the WFS is shown for a specific data set. The following remarks can be made:

- The cumulative variance clearly shows the presence of 'steps' at discrete frequencies for both telescope axis;
- the total equivalent single axis jitter is of the order of $30\,mas$;
- most of the residual is at higher frequencies and in particular the equivalent single axis jitter at frequencies below $20\,Hz$ is less than $10\,mas$.

It is clear that the residual tip-tilt jitter is not acceptable considering that the d.l. in $H-band$ is $54\,mas$ and in particular the measured residual 'explains' the large loss of Strehl in the long exposures. Unfortunately this residual is distributed at frequencies where the AO loop does not have any ability of correcting. In fact even at full speed given the delays in the loop the $0dB$ point of the error rejection function for tip-tilt is on the order of $20-25\,Hz$ (see Fig.8).

Based on measurements taken with accelerometers installed on the adaptive secondary we can conclude that most of these vibrations happen at the front end of the telescope. We were in fact able to identify most of the 'steps' in the cumulative variance with specific 'modes' of the telescope structure. We are therefore envisaging

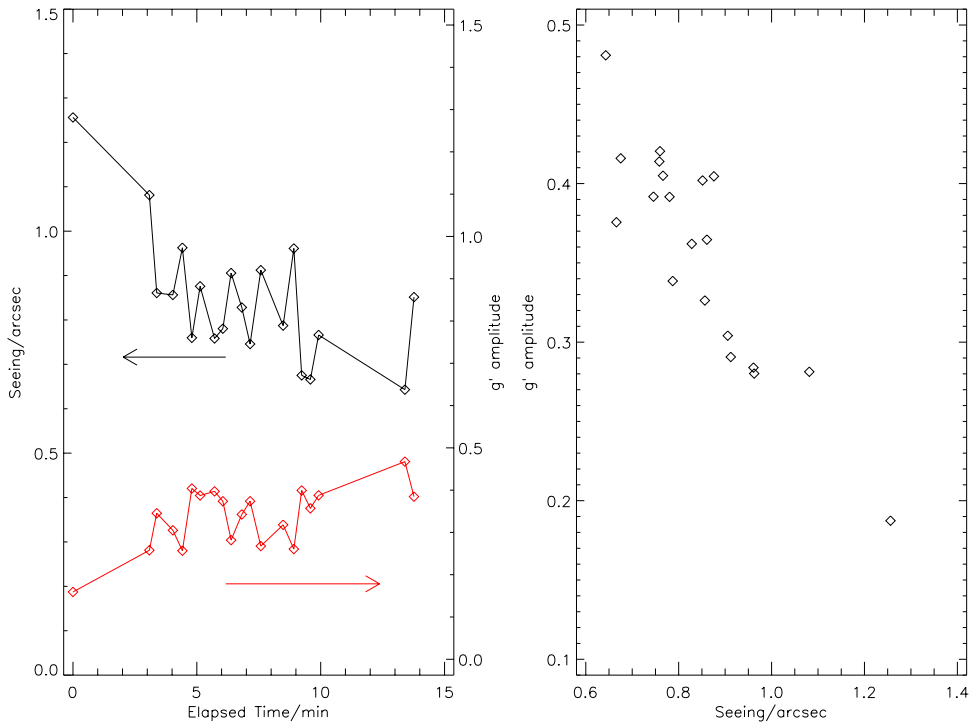

Figure 6. Effects of the seeing on the WFS gain $g^{'}$.(Left) seeing angle and $g^{'}$ amplitude as a function of time. The correlation between these quantities is evident. (Right) the same data are plotted against each other to show the relationship between them. These data were taken using several different modes for the modulation.

using the same accelerometers to feed-forward a tip-tilt signal directly to the mirror by-passing the AO loop to try to cancel these vibrations. The issues associated with this solution are the following:

- since this is essentially an open loop correction any mis-calibration between the coordinate system associated with the accelerometers and the system associated with adaptive secondary will results in a net error;
- because of the strong dependency of the electrical noise of accelerometers with frequency a low limit to the frequency must be set. This is around $10\,Hz$ if simple integrated three-axis accelerometers are used.

Finally, although the adaptive secondary time response for tip-tilt is quite short ($2-3\,ms$ settling time) this has to be taken into account at least for the high frequency end of the spectrum of vibrations.

6. CONCLUSIONS

The MMT-AO equipped with the first adaptive secondary ever developed has been successfully operated for almost two years. A total of seven runs have been accumulated so far. These runs have allowed us to build confidence in the adaptive secondary. During these runs we also have identified several important modifications that we will try to retrofit on this mirror and that will become the standard for future adaptive secondaries. In particular we mention a mechanism to retract the thin shell when the mirror in not powered which we are planning to implement soon. From a more general viewpoint we conclude that the MMT-AO system can be considered fully characterized for what concerns the operation with bright reference stars ($M_V \leq 10$) and some more work needs to be done to optimize the system for fainter reference stars. We also explored a new technique loosely called "reconstructor on the sky". Although this method has not yet been proven to produce a measurement of

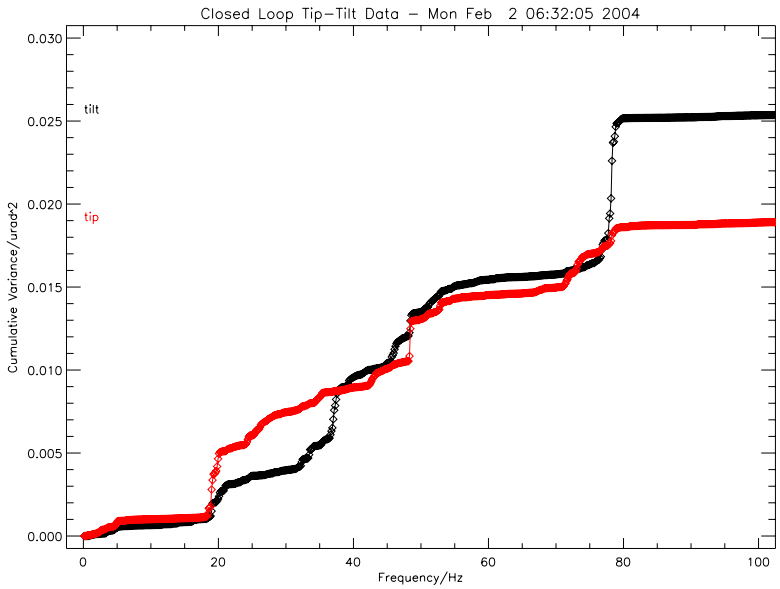

Figure 7. Closed loop cumulative variance of the tip-tilt signal as seen by the WFS. The steps correspond to peaks in the power spectrum. Most of the peaks have been identified as either mechanical resonant modes of the telescope structure or vibrations caused by the telescope control system.

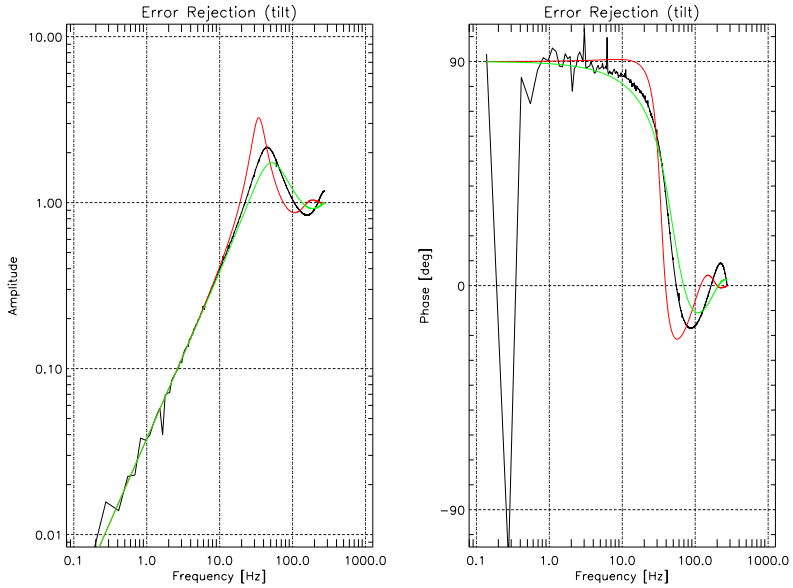

Figure 8. Error rejection function (Amplitude and Phase) computed from WFC data. The three curves represent: continuous model of the system response (highest peak), WFC data , response including only the WFS time delay (lowest peak). The actual system response is most likely between the two extremes and cannot more accurately determined given the precision with which the time jitter in the acquired data is known.

the system interaction matrix good enough for AO operation it has already shown to provide a measurement of the effect of the seeing on the overall system gain. This effect which is due to the fact that our SH WFS uses quad-cells to measure the sub-apertures centroid can in fact be measured directly with this technique.

ACKNOWLEDGMENTS

We would like to thank Richard Gonzalez-Sosa and Manny Montoya for their essential contribution both at the telescope and in the lab. We are also very thankful to the MMT crew for their patience and very valuable help. This work has been supported by the Air Force Office of Scientific Research under grant AFOSR#F49620-01-1-0383.

REFERENCES

1. A. Riccardi, G. Brusa, C. del Vecchio, P. Salinari, R. Biasi, M. Andrighettoni, D. Gallieni, F. Zocchi, M. Lloyd-Hart, F. Wildi, and H. M. Martin, "The adaptive secondary mirror for the 6.5 conversion of the Multiple Mirror Telescope," in *Beyond Conventional Adaptive Optics*, 2001.
2. G. Brusa, A. Riccardi, P. Salinari, F. P. Wildi, M. Lloyd-Hart, H. M. Martin, R. Allen, D. Fisher, D. L. Miller, R. Biasi, D. Gallieni, and F. Zocchi, "MMT adaptive secondary: performance evaluation and field testing," in *Adaptive Optical System Technologies II. Edited by Wizinowich, Peter L.; Bonaccini, Domenico. Proceedings of the SPIE, Volume 4839, pp. 691-702 (2003).*, pp. 691–702, February 2003.
3. G. Brusa, A. Riccardi, F. P. Wildi, M. Lloyd-Hart, H. M. Martin, R. Allen, D. L. Fisher, D. L. Miller, R. Biasi, D. Gallieni, and F. Zocchi, "MMT adaptive secondary: first AO closed-loop results," in *Astronomical Adaptive Optics Systems and Applications. Edited by Tyson, Robert K.; Lloyd-Hart, Michael. Proceedings of the SPIE, Volume 5169, pp. 26-36 (2003).*, pp. 26–36, December 2003.
4. D. Miller, G. Brusa, M. F. Kenworthy, P. Hinz, and D. Fisher, "Status of the NGS adaptive optic system at the MMT Telescope," in *this conference*,
5. M. A. Kenworthy, D. L. Miller, G. Brusa, P. M. Hinz, D. L. Fisher, M. Lloyd-Hart, F. P. Wildi, D. W. McCarthy Jr, D. L. Dylan, C. Kulesa, P. A. Young, B. D. Oppenheimer, W. Liu, M. R. Meyer, and J. Greissl, "Scientific results from the MMT natural guide star adaptive optics system," in *this conference*,
6. P. C. Mcguire, M. Lloyd-Hart, J. R. P. Angel, G. Z. Angeli, R. L. Johnson, B. C. Fitz-Patrick, W. B. Davison, R. J. Sarlot, C. J. Bresloff, J. M. Hughes, S. M. Miller, S. Schaller, F. P. Wildi, M. A. Kenworthy, R. M. Cordova, M. J. Rademacher, M. H. Rascon, J. H. Burge, B. L. Stamper, C. Zhao, P. Salinari, C. del Vecchio, A. Riccardi, G. Brusa, R. Biasi, M. Andrighettoni, D. Gallieni, C. Franchini, D. G. Sandler, and T. K. Barrett, "Full-system laboratory testing of the F/15 deformable secondary mirror for the new MMT adaptive optics system," in *Proc. SPIE Vol. 3762, p. 28-37, Adaptive Optics Systems and Technology, Robert K. Tyson; Robert Q. Fugate; Eds.*, **3762**, pp. 28–37, September 1999.
7. N. Takato, M. Iye, and I. Yamaguchi, "Wavefront reconstruction error of Shack-Hartmann wavefront sensors," *Pub. Astr. Soc. Pac.* **106**, pp. 182–188, February 1994.